Ab-initio study of the optical properties of beryllium-sulphur co-doped graphene

Cite as: AIP Advances 9, 025221 (2019); doi: 10.1063/1.5060708
Submitted: 21 September 2018 • Accepted: 18 February 2019 •
Published Online: 27 February 2019

O. Olaniyan, E. Igumbor, A. A. Khaleed, A. A. Mirghni, and N. Manyala[a)]

AFFILIATIONS

Dept. of Physics, Institute of Applied Materials, SARCHI Chair in Carbon, Technology and Materials, University of Pretoria, 0028, South Africa

[a)]**Corresponding author's email:** ncholu.manyala@up.ac.za; **Tel.:** +(27)12 420 3548; **Fax:** +(27)12 420 2516

ABSTRACT

Graphene is a carbon material with excellent properties, which makes it applicable in a myriad of applications. However, the range of the applications of graphene can be extended to the developing field of nanoelectronics and optoelectronics by doping it with heteroatoms. In this study, Be and S atoms were used to co-dope graphene. The impurity concentration was varied by increasing the size of the supercell from 2x2 through 4x4. First-principles calculations were performed to determine the dynamic stability, band structure, and optical characteristics of the system. The results of the phonon dispersion of beryllium and sulphur co-doped graphene (Be-S) show the absence of imaginary modes, suggesting that Be-S is dynamically stable. The analysis of the band structure indicates that it has a tunable indirect band-gap which increases with the impurity concentration. A band-gap magnitude is required in a graphene-based transistor. Thus, Be-S could be considered as a transistor material. As regards with the optical properties, it is observed that the optical transparency of the graphene in the ultraviolet region changes with the impurity concentration. The result shows that Be-S can be used to manipulate light waves for a device application.

I. INTRODUCTION

Graphene is a single layer of sp^2 hybridized carbon atoms packed in a honeycomb lattice. The outstanding properties (such as high carrier mobility,[1–4] exhibitions of ballistic transport,[5] high tensile strength,[6] high flexibility, high thermal conductivity,[7] and ambipolar field effect[8]) make it a promising material for use in nano-electronic and optoelectronic devices. However, graphene has a zero band-gap,[8–10] high sheet resistance,[11–13] and these make it difficult for direct integration into nano-devices. The substitutional doping of graphene with heteroatoms has extensively been studied as an effective technique for creating a sizeable band-gap or tailoring the sheet resistance[14] of the material. In general, different heteroatoms doped graphene have been investigated either experimentally or theoretically. In the present study, we explored the potential application of graphene-based material in nano-devices by co-doping.

There are several reports on heteroatoms doped graphene and could be considered as the basis for the present study. Heteroatoms doping of graphene via substitution means an act of replacing a number of carbon atoms of graphene with the elements (other than carbon and hydrogen atom) in the periodic table. Nath et al.[15] performed a first-principles study to determine the electronic structures of boron (B), nitrogen (N), B and N co-doped graphene (B-N). They remarked that the induced direct band-gaps in the doped systems varied with the impurity concentration. Moreover, in the long wavelength limit, the optical parameters of the doped systems (with respect to the parallel polarisation of the field vector) were modified with the impurity concentration. However, they did not calculate the phonon dispersion of the systems to determine if the systems are dynamically stable. Similarly, but in a separate study, Rani et al.[16] employed density functional theory (DFT) to investigate the frequency dependent optical characteristics of B, N doped graphene and B-N. They arrived at the same conclusion as Nath et al.[15] In addition, they indicated that the absorption peaks of the B-N were red-shifted towards the visible regime as the impurity concentration increases. However, regardless of the impurities percentage in graphene, their results suggest that the B-N remains transparent in the UV region. In another study[17] pertaining to the electronic structure of the B-N, the size of the direct band-gap was observed to depend on the choice of the sublattice points that the co-dopants

occupied in graphene. However, the report did not considered the effect of the sublattices occupied by the impurities on the optical properties of graphene. Recently, DFT was employed to study the effects of B, N concentration and the doping sites on the band-gap of graphene.[18] The results show that the energy gap of the doped system depends on the defects concentration and the doping pattern. However, the lattice dynamics study of the systems was done to ascertain which pattern of doping is dynamically stable. More recently, Mann et al.[19] studied the thermodynamic properties of graphene doped separately with B and N. They remarked that the dynamic stability and the specific heat capacity of the system decreased with the impurity concentration.

Although N and B atoms are the ideal substitutes for carbon atoms of graphene, due to the size of their atomic radii which are almost the same as that of the carbon atom, other light elements like beryllium and sulphur have also been investigated. Beryllium electronic configuration is $1s^2\ 2s^2$, which in the current form, appears not to favour the formation of covalent bonds with the carbon atoms of graphene. However, the electron in 2s could be partly promoted to 2p orbitals (since the energy interval between the two orbitals is small) leading to a substantial orbital mixing or hybridisation, and as a result seems to favour the formation of covalent bonding. Consequently, Ferro et al.[20] investigated the adsorption of Be atoms on monolayer and bilayer graphene, and realised that the dopants were more weakly bonded to a monolayer compared to the bilayer graphene. It was stated that Be_2 could form magnetic or non-magnetic structures on graphene depending on the conformation of the adsorbates. However, the optical characteristics of the systems were not studied. Ullah et al.[21] reported on the geometric structure and the electronic characters of Be doped graphene, Be and B dual doped graphene (Be-B). They argued that, with a rectangular doping, a 12.5% impurity concentration would induce maxima band-gaps of 0.99 and 1.44 eV in Be-B and Be doped graphene, respectively. However, they did not report the effect of the impurities on the optical properties of the systems. Hussain et al.[22] studied the geometric structure and the electronic properties of Be and N co-doped, and Be-O molecule-doped graphene. They revealed that the increase in the impurity percentage in graphene does not always lead to a band-gap enhancement. However, they, likewise, did not report the optical properties of the systems or the dynamic stability to show that the systems investigated have no imaginary modes. In another study, Denis et al.[23] investigated the effects of sulphur substitution on single-walled carbon nanotubes and graphene from first principles. They remarked that, in the case of doped graphene, the defects could either induce a semiconducting or metallic character in graphene depending on the sulphur content. However, they did not investigate the effect of heteroatoms co-doping as an avenue to eliminate the metallic character of the system. Recently, we studied the geometric structure and electronic properties of the in-plane beryllium and sulphur co-doped graphene (Be-S) at a fixed impurity concentration. We observed that the band-gap of the Be-S depend on the relative positions between the impurities in the system.[24] However, in the study, the out-of-plane conformation of the defects in graphene was not taken into consideration to determine if it is more stable than the in-plane configuration. Moreover, the impurity concentration effect on the lattice dynamics, electronic and optical characteristics of the system were not studied as well.

Despite the numerous studies that have been done with ab-initio calculations to predict the properties of heteroatoms doped graphene, synthesising such heavily doped (i.e. with the impurity concentration above 5%) nanostructures experimentally remains a contending issue. As a result, other heteroatoms doped graphene are being explored to determine if they would be amenable for synthesis experimentally at a higher impurity concentration. In view of the above, we report for the first time the effects of the atomic pairs of Be and S on the dynamic stability, electronic and optical properties of graphene. Moreover, in the study, the in-plane and out-plane substitution of the Be and S atoms in graphene were evaluated to determine how the impurities prefer to co-exist in graphene. It is expected that the result of this study would provide an insight into the realisation of graphene-based nano-devices.

II. METHODS

The electronic structures and optical characteristics of calculations Be-S were performed from first-principles within the scoped of DFT as implemented in the Vienna Ab-initio Simulation Package (VASP).[25–28] In the simulations, the Projected Augmented Wave (PAW) was employed to model the system of the ion-electron interactions, while the Perdew Burke Ernzerhof (PBE) generalised gradient approximation (GGA)[29] was used as the exchange-correlation functional. To improve on the usual underestimation of energy band-gap by semi local functionals, we used HSE06.[30] The lattice symmetry of graphene can be broken if it is co-doped with dopants with larger molecular radii than carbon atom. Consequently, more high symmetry K-points in the Brillouin zone (BZ) (as shown in Fig. 1) must be sampled in order to obtain an accurate plot of the band structure of the co-doped system. Based on this, the path

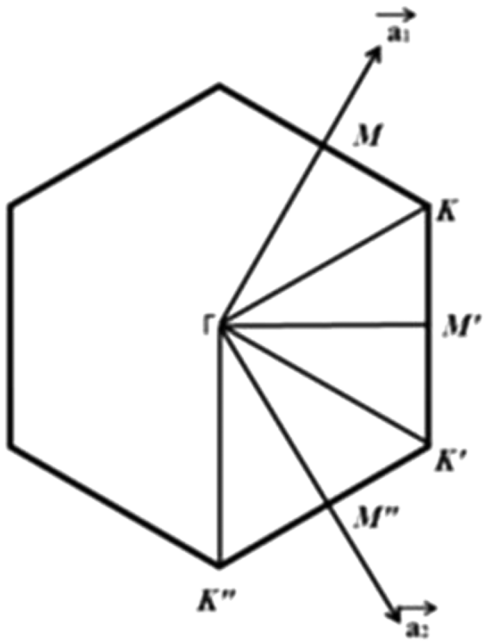

FIG. 1. The path between the high symmetry points in the BZ for the calculation of the band structure of Be-S.

in the BZ via which the band structures of Be-S was calculated is given through Γ–M–K–Γ–M′–K′–Γ–M′′–K′′–Γ sampling route. Kohn-Sham orbital expansions with the plane-wave basis set were done with the kinetic energy cutoff (Ecut) of 400 eV, and the convergence criterion of 10^{-5} eV was used for the computations of all the systems that were studied. The systems that were studied consist of 8, 18 and 32 atoms corresponding to periodic slabs of 2x2, 3x3 and 4x4 supercell of graphene co-doped with an atomic pair of beryllium (Be) and sulphur (S). To avoid the interlayer interaction between a layer of graphene and the periodic image, a test of convergence with respect to vacuum spacing was done.

A vacuum size of 14 Å along with the periodic boundary conditions was observed to give a converged result when applied between any two adjacent layers of graphene. Geometrical relaxation of all the systems was done such that the Hellmann-Feynman forces is less than a predetermined threshold value of 0.002 eV $Å^{-1}$. For Brillouin zone (BZ) sampling, a Γ–centred grid of 13 k ×13 k ×1k-mesh was used. For the integration scheme, Gaussian smearing with 0.2 eV width was used for the self-consistent field calculation (scf). The formation energy E_f requires for a defect to form in graphene was calculated as follows:

$$E_f = E_d - \sum_t n_t \mu_t \tag{1}$$

where E_d denotes the energy per unit cell of graphene with impurities; the subscript 't' denotes the index of summation of the set of atoms of a particular type; whereas the number of a set of atoms of type 't' is represented as n_t, the chemical potential associated with atoms of type "t" is represented as μ_t. Carbon chemical potential μ_c was calculated as the total energy of graphene divided by the number of the carbon atom in the unit cell. So that the formation energy of defect-free graphene is equal to zero. To compute the sulphur (S) chemical potential μ_S, the energy per unit atom obtained from the crystalline S with a face-centred orthorhombic lattice (space group of Fddd) was used. For Be, the hexagonal crystalline lattice was employed to compute the chemical potential μ_{Be}.

It is worth mentioning that during the geometry optimization of Be-S, spin and unspin polarized calculations were performed. The results of the two computations have the same energy, with the resultant zero magnetic moments. Consequently, the unspin polarized calculations were applied to the remaining systems to save computational cost.

The optical characteristics of Be-S were calculated with the dielectric function $\varepsilon(w)$ (equation 2); where the imaginary part ε_2 was computed employing first-order time-dependent perturbation theory in the basis of simple dipole approximation. The changes in the periodic part of the potential, known as the local field effects, have been included within random phase approximation (RPA).

$$\varepsilon(\omega) = \varepsilon_1(\omega) + i\varepsilon_2(\omega) \tag{2}$$

In the long wavelength limit, the imaginary part of the complex dielectric function could be expressed as:

$$\varepsilon_2(q \to 0, \omega) = \frac{2e^2\pi}{V\varepsilon_0} \sum_{c,v,k} |\langle \psi_k^c | \vec{u} \cdot \vec{r} | \psi_k^v \rangle|^2 \delta(E_k^c - E_k^v - \omega) \tag{3}$$

where 'c' and 'v' are the band indices corresponding to the conduction and valence bands; V and ε_o represent the unit cell volume and the free space permittivity, respectively. ω (expressed in eV) is a particular frequency of the incident electromagnetic wave (EM). In this order, $\vec{u}$ and $\vec{r}$ denote the incident EM wave polarization vector and the position vector. At a k-point, the eigenfunctions corresponding to the valence and conduction bands of the given systems are represented by ψ_k^v and ψ_k^c, respectively. The E_k^c and E_k^v correspond to the eigenvalues.

The real component of the $\varepsilon(w)$, ε_1 is calculated from ε_2 employing the Kramers-Kronig transformation:

$$\varepsilon_1(\omega) = \mathrm{Re}[\varepsilon(q \to 0)] = 1 + \frac{2}{\pi} P \int_0^\infty \frac{d\omega' \varepsilon_2(\omega')\omega'}{\omega'^2 - \omega^2 + i\eta} \tag{4}$$

where P stands for the Cauchy principal value. The technique has been reported in Ref. 31. It is worth noting that ε_1 and ε_2 have two independent parts which are the two polarizations of the EM field with respect to the plane of the materials. These two polarizations are called the parallel (the polarised vector is along the plane of the system) and the perpendicular (the polarised vector is out of the plane of the system) polarization in this study. It is worth mentioning that equation (3) has no Drude component. Drude term accounts for the intraband transition which is dominant at the low energy.

Given the data sets of $\varepsilon(\omega)$, the optical characteristics of the graphene and Be-S were calculated using equation (5) through (9):

$$n(\omega) = \left(\frac{\sqrt{\varepsilon_1^2 + \varepsilon_2^2} + \varepsilon_1}{2} \right)^{\frac{1}{2}} \tag{5}$$

$$k(\omega) = \left(\frac{\sqrt{\varepsilon_1^2 + \varepsilon_2^2} - \varepsilon_1}{2} \right)^{\frac{1}{2}} \tag{6}$$

where $n(\omega)$ is the real and $k(\omega)$ is the imaginary part of the complex refractive index $\tilde{u}$ with the relation, $\tilde{u} = n(\omega) + ik(\omega)$. The equations (5) and (6) were used to calculate the reflectivity R of the systems of study provided the incident polarized EM is perpendicular to the plane of the samples.

$$R(\omega) = \frac{(n-1)^2 + k^2}{(n+1)^2 + k^2} \tag{7}$$

The absorption coefficient $\alpha(\omega)$ of the systems was computed with the equation (6) above

$$\alpha(\omega) = \frac{2k\omega}{c\hbar} \tag{8}$$

where "c" of equation. (8) represents the velocity of EM field in the vacuum. The remaining variables retain the same descriptions as earlier declared.

$$L(\omega) = \frac{\varepsilon_2}{\varepsilon_1^2 + \varepsilon_2^2} \tag{9}$$

The measure of the collective excitation of a given system is expressed by the electron energy loss function $L(\omega)$ and could be calculated by applying equation (9). The quantity can be derived from $\mathrm{Im}(-1/\varepsilon(q \to 0, \omega))$ and the magnitude of the value increases as $\varepsilon_1 \to 0$ and $\varepsilon_2 < 1$ at the plasma frequency. To evaluate the optical constants of the Be-S and the graphene, a considerable number of empty bands were applied in the calculations. Additional empty bands were included in our optical calculations to account for high-frequency interband transitions.

For the study of the lattice dynamics of the systems, the direct method[32] was used within the limit of the harmonic approximation.

III. RESULTS AND DISCUSSION

A. Formation energy

The formation energy per unit cell E_f of a solid could be employed to access the stability and the relative tendency of such system to be synthesized in the laboratory. As a result, in this study, E_f of pristine and Be-S was calculated with the equation (1). To calculate the E_f of pristine graphene, the system was first geometrically optimised. After the relaxation, 2.46, 1.42 Å (see Fig. 2a) and 0 eV were realised as the lattice constant, C–C bond length and E_f of the system respectively. The calculated values of the lattice parameters are in close agreement with the existing theoretical[21] and experimental[9,33] reports. Therefore, the agreement between these results and the literatures validates the computational method adopted in this study. Meanwhile, as earlier stated, the E_f of the defect-free graphene is zero because the chemical potential of the carbon atom was calculated using pristine graphene (not graphite) as the reference. The advantage of zeroing the E_f of graphene is that the relative stability of a doped graphene system could easily be compared. This suggests that a doped graphene system with $E_f > 0$ has lower stability than pristine graphene. Moreover, the converse of this statement also holds for $E_f < 0$.

Next, the E_f of Be-S was evaluated to determine how the defects prefer to co-exist in graphene. In our earlier report,[24] it was demonstrated that Be and S atoms prefer to replace in-plane C–C of graphene. In the study, it is argued that the favourable predisposition of Be to S bonding in graphene is as a result of the formation of the ionic bonding between the defects. However, in the report, the out-of-plane substitution of the impurities was not taken into account in order to determine if it is energetically more favourable than the in-plane substitution. In the present study, the two conformations were accessed to determine which one is more favourable to be experimentally synthesised. The two conformations are shown in Fig. 2 [(b) and (c)] and they correspond to the in-plane and the out-of-plane substitution of Be and S for the carbon atoms in a 2x2 supercell of graphene, respectively. From the results of the formation energies, it is found that the out-of-plane substitution of Be and S atomic pair in graphene is energetically more favourable than the in-plane substitution of the defects. The lower value of the E_f of the Be-S co-doped graphene might be attributed to the fact that the atoms of the system have a tendency to be densely more packed in the out-of-plane than the in-plane arrangement thereby reducing the amount of stress experiences by the system. Consequently, in the rest of this study, the out-of-plane conformation was employed whenever the atomic duo of Be and S were substituted for the carbon atoms of graphene. Fig. 2 [(d) and (e)] show a 3x3 and a 4x4 Be-S systems which correspond to 11.0 and 6.3% impurity concentrations respectively. The supercells of the systems were varied purposely to induce the different amount of the defects in graphene. Table I gives the summary of the different amount of the defects created in graphene and the corresponding E_f.

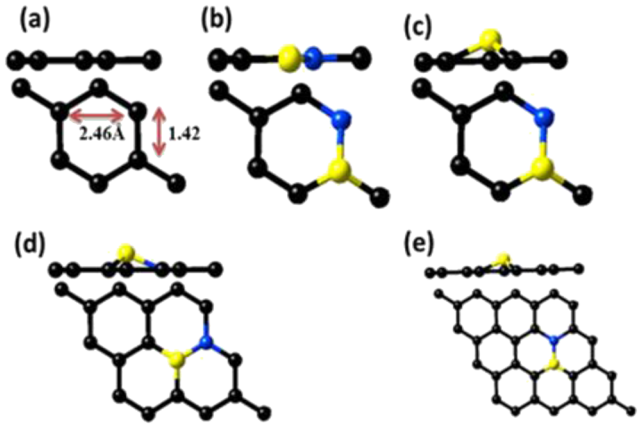

FIG. 2. The optimised geometry of Be-S with (a) 0% (b) 25% (in-plane) (c) 25% (out-of-plane) (d) 11% (e) 6.3% (out-of-plane).

B. Dynamic stability of Be-S

In order to establish the dynamical stability of Be-S, the lattice vibrational modes of the least stable B-S (with 25% impurity) were investigated using the harmonic approximation. Table I shows that the E_f of the Be-S increases with the defects concentration. For instance, the pristine graphene is the most stable with 0 eV as the E_f, while 4.85 eV is for Be-S with the 25% impurity concentration. Due to the expensive nature of phonon calculations, in the present study, only the vibrational modes of the least stable structure of Be-S co-doped system along with that of pristine graphene were investigated.

The calculation of the phonon curve of pristine graphene was done with a 1x1 supercell which contained two carbon atoms. The result of the calculation is displayed in Fig. 3(a). Six phonon modes can be seen and they correspond to the three optical (LO, TO, ZO) and acoustic (LA, TA, ZA) branches. The LO, TO and ZO tags on the curve represent the longitudinal, transverse and optical branches, respectively. The corresponding acoustic components are labelled as LA, TA, and ZA. Some of the key values of the curve at high symmetry points are tabulated in Table II. According to Table II, it is interesting to observe that the values are quite in agreement with the existing theoretical[35] and experimental[34] reports on the phonon dispersion curve of the pristine graphene. The close agreement between this result and the existing literature accedes to the reliability of the computational method employed in this work.

Following the validation of the computation method, the technique was subsequently applied to calculate the phonon spectrum curve of Be-S with a 25% impurity concentration. The system was

TABLE I. The relationship between the impurity concentration of Be-S and the E_f.

Impurity concentration (%)	Systems+Supercells	E_f (eV)
0	Pristine graphene 2x2	0
6.3	Be-S 4x4	4.14
11.0	Be-S 3x3	4.22
25.0	Be-S 2x2	4.85

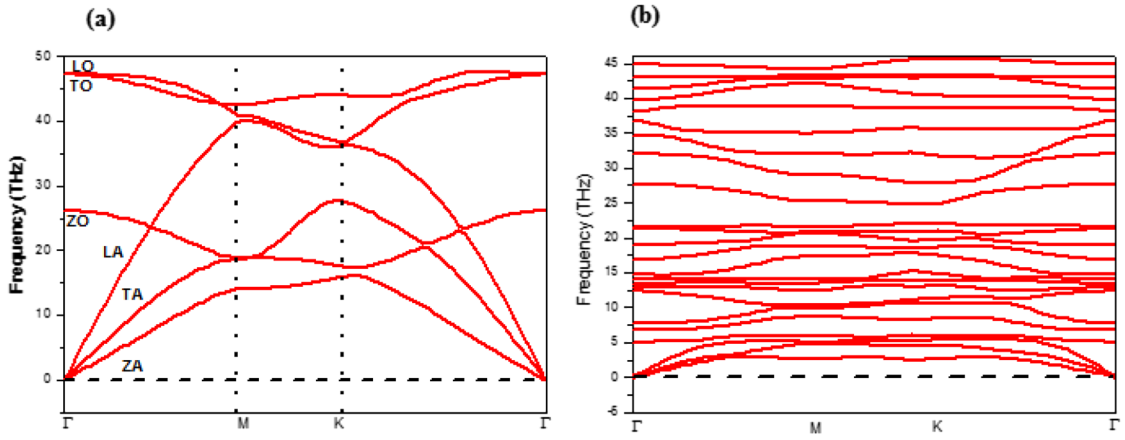

FIG. 3. Phonon dispersion curve of a (a) 1x1 supercell of pristine graphene (b) 2x2 supercell of Be-S with a 25% defect concentration. LO (LA), TO (TA), ZO (ZA) are the longitudinal, and transversal (optical) branches.

optimized until the forces on all the atoms were less than 0.002/Å. Fig. 3(b) shows the phonon spectrum of Be-S with a 25% impurity concentration. It is worthwhile to note that the absence of imaginary modes on the curve is an indication that the system is dynamically stable, and as a result, it is amenable for synthesis in the laboratory if the necessary precursors are used.

C. Band-gap tuning of graphene

The electronic band-gap of Be-S with different impurity concentration was studied and compared with that of the pristine graphene. It is shown in Fig 4(a) that the pristine graphene is a gapless nanomaterial as a result of the touching of the minimum conduction and the maximum valence band at the K-point of the BZ. The π and π^* states form the valence and the conduction bands respectively. At the low energy region, the band has a linear relation and the band structure could be seen as two cones meeting at the Dirac point. The touching of the bands at the neutrality point indicates that graphene has no band-gap. The zero band-gap in graphene is as a result of the similar background of the two carbon atoms in the 1x1 unit cell of graphene. These basic features of the band structure of pristine graphene are in agreement with the earlier studies.[9,10,36]

TABLE II. Computed phonon frequencies at Γ, M, K, Γ point in the BZ of graphene.

	present study	theoretical	experimental
high-symmetry points	GGA (PBE) (in THz)	Ref. 35 (in THz)	Ref. 34 (in THz)
Γ_{ZO}	26.14	26.41	26.02
Γ_{LO}	47.23	46.58	47.36
Γ_{TO}	47.23	46.58	47.36
M_{ZA}	13.78	14.12	13.52
M_{LA}	39.70	39.81	39.81
M_{ZO}	19.02	19.03	19.03
M_{TO}	41.69	41.67	41.67
K_{ZA}	15.68	16.03	15.49
K_{ZO}	17.30	16.03	17.62
K_{LA}	36.32	36.36	36.36
K_{TO}	38.26	38.61	38.61

However, a band-gap can be induced in graphene if the two atoms in the unit cell could be made to co-exist at a different potential. Doping of graphene with an impurity induces energy gap in the system. Moreover, with a certain doping pattern, the size of the gap often depends on the amount of the impurity concentration incorporated into graphene.[18] For example, the effect of the Beryllium or sulphur concentration on the electronic structure of graphene has been done in separate studies.[21,23] In the case of Be-doped graphene, it is stated that the band-gap could be tuned as a function of the impurity concentration. In our recent study,[36] we have undeniably confirmed this to be true. However, at a high Be concentration, besides the material being dynamically unstable, we also found that the nanostructure formed a degenerate semiconductor. A degenerate semiconductor is a material with both metallic and semiconducting character. In another study, P.A. Denis *et al.*[23] have demonstrated that heavily S doped graphene exhibits a metallic character. Against this backdrop, in the present study, it is shown in Fig. 4 ((b)–(d)) that an atomic pair of Be and S could induce a tunable indirect gap of 0.72 eV (0.37 eV with GGA) in graphene. The system has a minimum indirect bang-gap of 0.20 eV at 6.3% while 0.72 eV is observed at 25% impurity concentration. Table III shows the summary of the result. Moreover, Be-S could be touted as a nanostructure with no metallic character since the Fermi level is right within the band-gap irrespective of the impurity concentration. The key factor that keeps the Fermi level within the energy gap of the system could be attributed to the isoelectronic nature of Be and S with regard to the pristine graphene. It is worth mentioning that in microelectronics, the smallest band-gap of 0.4 eV is required for a transistor to work in ON/OFF mode. Thus, the calculated magnitude of the band-gap of Be-S satisfies this requirement.

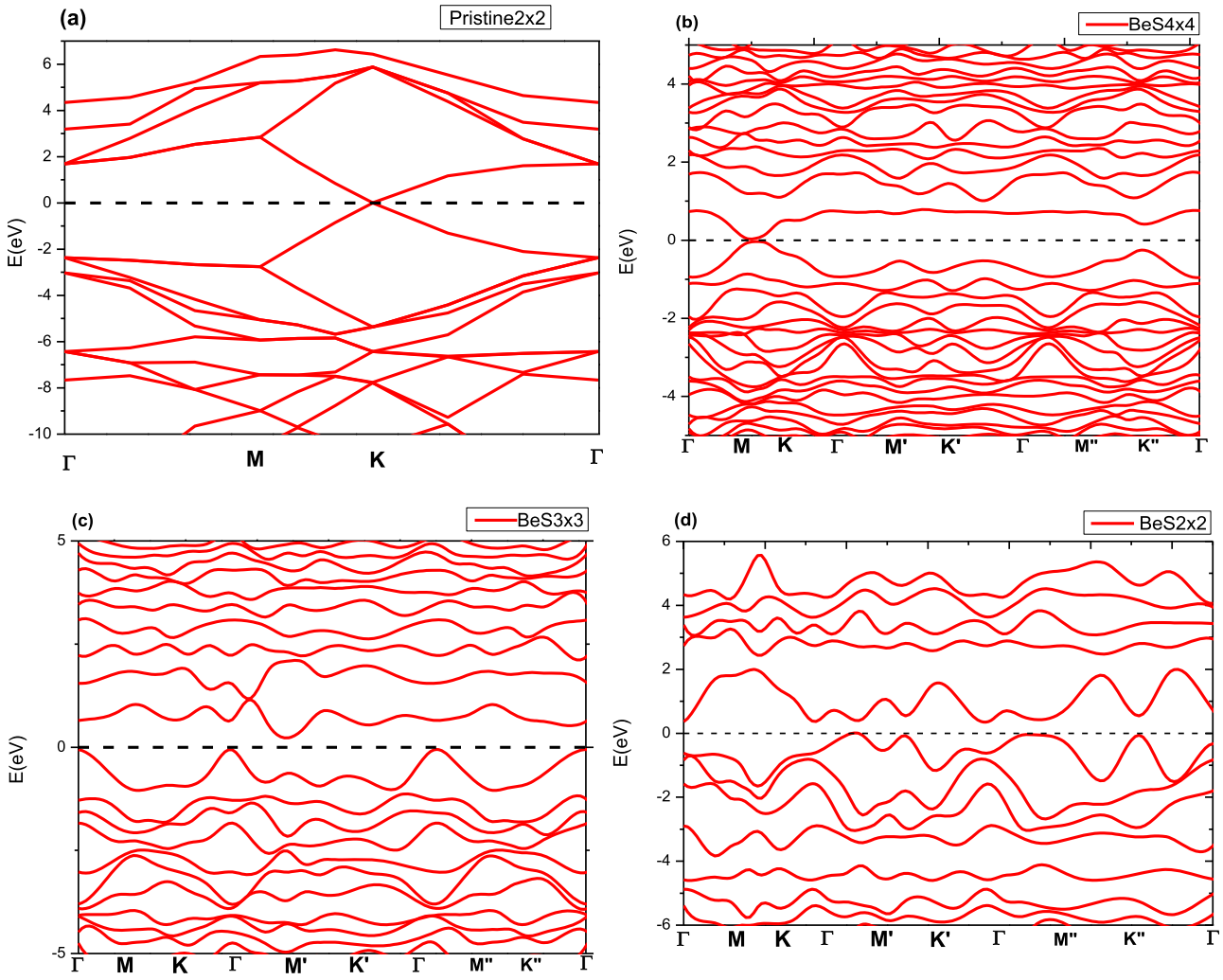

FIG. 4. Band structure of Be-S with a (a) 0% (b) 6.3% (c) 11% and (d) 25% impurity concentration.

D. Dielectric function

In the previous section, it was simply demonstrated that if graphene is co-doped with the atomic pair of Be and S atoms, the electronic band structure would be induced with the impurities dependent band-gap. Consequently, changes in the electronic structure of graphene are expected to result in the modification of the optical characteristics of the system. In this section, the effect of the impurity concentration of Be and S on the optical properties of pristine graphene has been studied. The discussion of the optical properties of the systems of interest is centred on the optical parameters like the dielectric function, refractive indices, reflectivity, absorptivity, and electron energy loss function (eels). Fig. 5 (a) and (b) show imaginary dielectric spectra of pristine (magenta colour), and co-doped graphene at different impurity concentrations (red, green and blue colour) with respect to the light polarisation vectors. The red spectrum is associated with a 2×2 supercell of graphene doped, via substitution, with a pair of Be and S to forms a 25% impurity concentration.

The green spectrum is associated with a 3×3 supercell of graphene doped with a pair of Be-S and corresponds to a 11.0%

TABLE III. The magnitude of the bandgap induced in graphene versus the impurity percentage.

System	defect conc.(%)	Band-gap (in eV) GGA (PBE)	HSE06
Pristine graphene	0	0	0
	6.3	0.08	0.2
Be-S co-doped graphene	11.0	0.28	0.63
	25.0	0.37	0.72

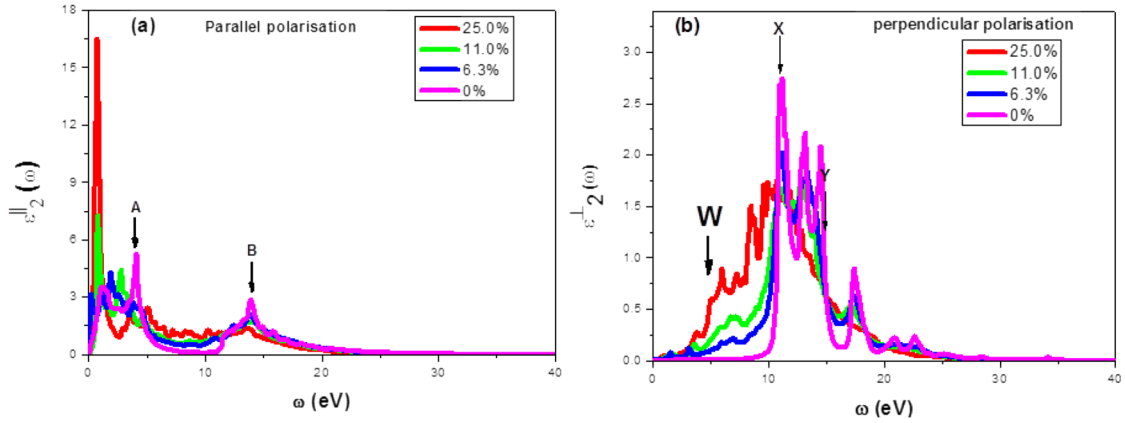

FIG. 5. The anisotropic imaginary dielectric spectra of graphene (magenta) and Be-S (blue, green, and red colour correspond to a 6.3, 11.0 and 25% impurity concentration) for (a) parallel polarisation (b) perpendicular polarisation of the electric field vector.

impurity concentration. The blue colour corresponds to 4×4 supercell of graphene with a 6.3% impurity concentration. The dielectric function has two different components denoted as $\varepsilon_2^{\|}$ and $\varepsilon_2^{\perp}$ which correspond to the polarisation of EM field vectors relative to the plane of graphene and would be described as parallel and perpendicular polarisation. These notations have also been extended to other optical parameters in this study.

With respect to the parallel polarisation of the electric field vector ($E_{\|}$), Fig. 5 (a), the imaginary dielectric curve of graphene is characterised with two prominent peaks. The first one (**A**) covers low-frequency regime up to 5.0 eV arising from intraband and interband transition with an intense peak at 4.0 eV whereas the second peak (**B**) with a wider frequency range, as a result of mainly interband transition, has a pronounced peak at 14.0 eV. Sandwiched between the two peaks of the spectrum is a featureless region stretching between 7.5-10.6 eV and has nearly zero intensity. The corresponding frequency of the two peaks is in excellent agreement with previous studies.[36-38] Recent spectroscopic ellipsometry study of graphene on amorphous quartz shows a distinct absorbance peak at 4.6 eV.[39] The higher value obtained from the experiment as compared to the first peak of our study could be ascribed to the neglect of the interaction between the substrate and the graphene sheet in our calculation. The basis of the peak **A** is attributed to the $\pi \rightarrow \pi^*$ transition on the line between M and K of the BZ (see Fig. 4 (a)) while the peak at **B** could be ascribed to $\sigma \rightarrow \sigma^*$ transition on the symmetry line between Γ and M (see Fig. 4 (a)) and this arises mainly from interband transition. Next, the effect of the atomic pair of Be and S atoms on the optical spectrum of graphene was observed with respect to the same electric field polarisations. As the percentage of the impurities increases, the height of peak **B** was noticeably reduces, whereas the peaks at **A** are red-shifted towards lower energy photon (see Fig. 5 (a)).

For perpendicular polarisation of the electric field ($E\perp$), as shown in Fig. 5 (b), the $\varepsilon_2^{\perp}$ spectrum of graphene has two contrasting peaks at 11.2 and 17.4 eV which are indicated as **X** and **Y**, respectively. With respect to $E\perp$, the dipole selection rule for the polarisation only allows the $\pi \rightarrow \sigma^*$ and the $\sigma \rightarrow \pi^*$ transitions. Thus, the basis of the peaks at **X** and **Y** in Fig. 5 (b) could be attributed to the $\pi \rightarrow \sigma^*$ and the $\sigma \rightarrow \pi^*$ interband transitions. Between 0 and 10 eV, we observed that the spectrum has zero intensity. This is because $\pi \rightarrow \pi^*$ transition with low energy resonance is forbidden as prescribed by the selection rule. Next, the effect of the impurity concentration on the graphene spectrum was considered. As the impurity concentration increases, it can be seen that the range of the energy frequency of the transition due to the peak **X** also increases while the intensity of the peak at **Y** decreases accordingly (see Fig. 5(b)). It is important to remark that while the $\varepsilon_2^{\perp}$ spectrum of graphene has nearly zero intensity between 0 and 10 eV, that of the Be-S increases with the amount of the impurities within the given frequency interval. The change in the amplitude of $\varepsilon_2^{\perp}$ spectra of Be-S, within 0-10.0 eV, as a result of the defect concentration is indicated with the black arrow and designated as **W** in Fig. 5 (b).

The ε_1 of pristine and Be-S co-doped graphene was computed using Kramers-Kronig transformation (see Eq. 4) for both $E_{\|}$ and $E\perp$. Fig 6 (a) and (b) depict the $\varepsilon_1^{\|}$ and $\varepsilon_1^{\perp}$ spectra respectively of the pristine along with Be-S co-doped graphene at different impurity concentration. With regard to $\varepsilon_1^{\|}$ (Fig. 6 (a)), pristine graphene has a prominent peak in the region of 0-4 eV, a minimum near 5 eV and a broader peak with maximum intensity at 11.3 eV. The features of this spectrum and the exact position of the peaks are in good agreement with the existing theoretical and experimental reports.[15,40] For Be-S, it is remarkable to note that the intensity of the spectrum of the system, within the region 1.0-15.0 eV, approaches that of pristine graphene as the percentage of the impurity decreases. For instance, in Fig. 6 (a) around **M** and **N** point, it can be observed that the intensity of the features of Be-S co-doped graphene tends to that of pristine as the impurity concentration decreases.

In the following discussion, the $\varepsilon_1^{\perp}$ spectrum of pristine graphene is compared with that of Be-S at different impurity concentrations. (Fig. 6 (b)) shows the spectrum of graphene with a pronounced peak at 11.0 eV, a minimum at 15.0 eV and the features are highlighted as **R** and **S**. Next, the effect of the atomic pair of Be-S on the optical spectrum of graphene was studied. Between 0-11 eV it is observed that $\varepsilon_1^{\perp}$ curve of Be-S approaches that of pristine graphene as the impurity percentage reduces from 25% to 6.3%. A similar behaviour of the spectrum of Be-S in relation to graphene is noticeable at 15.0 eV.

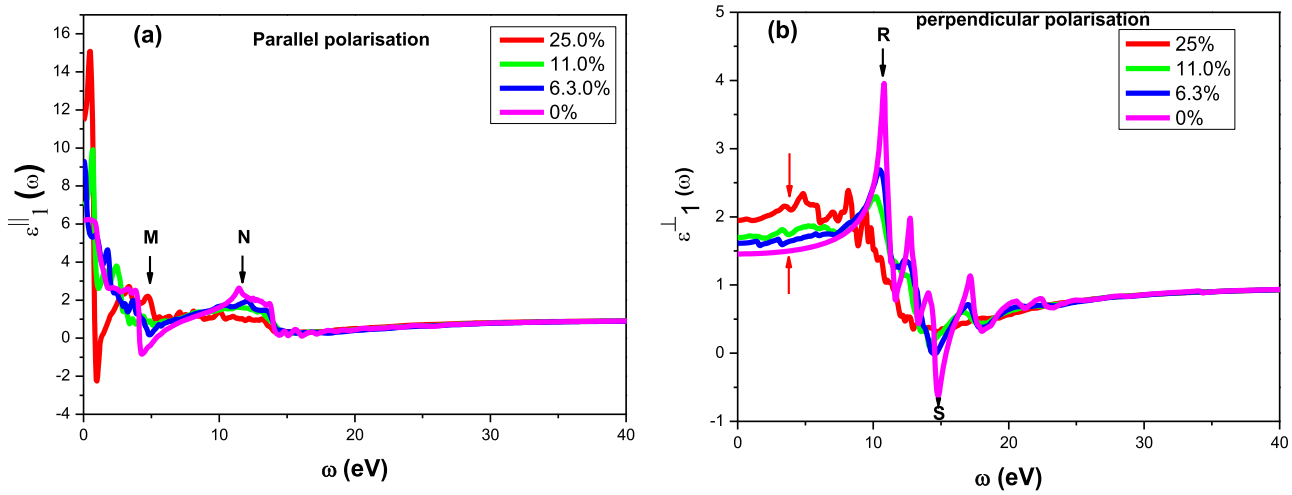

FIG. 6. The anisotropic real part of the dielectric spectra of graphene (magenta) and Be-S (blue, green, and red colour correspond to a 6.3, 11.0 and 25% impurity concentration) for (a) parallel polarisation (b) perpendicular polarisation of the electric field vector.

E. Absorptivity

Graphene is an outstanding system with excellent optical properties arising from its unique electronic structures. It can absorb light from the visible to infrared region of the electromagnetic spectrum. The absorption spectrum of the system arises from an intraband transition (at a low energy frequency within the far-infrared region) and an interband transition (at a higher energy frequency in the mid-infrared to the ultraviolet range).

Fig. 7 shows the absorption spectra of graphene and Be-S with the different impurity concentration in relation to $E_{||}$ and $E\perp$. As regards to $E_{||}$ spectrum, pristine graphene has two pronounced peaks (see Fig. 7 (a)). The first peak is located at 4.2 eV and is due to the $\pi\rightarrow\pi^*$ transition through M-K route in the Brillouin zone (see Fig. 4(a)). The transitions leading to the peaks are composed of the first valence band under the Fermi level to the first conduction band at the top of the Fermi level. However, the second peak occurs at 14.0 eV as a result of the $\sigma\rightarrow\sigma^*$ transition which is dominated by the second valence state under the Fermi level to the second conduction state at the top of the Fermi level. In addition to this, the system has a featureless region (between **A** and **B** point) which exists within the interval of 7.0-10 eV where the absorption coefficient of pristine is almost equal to zero. It worth pointing out that the features of this spectrum are consistent with the existing reports[16,36,41]

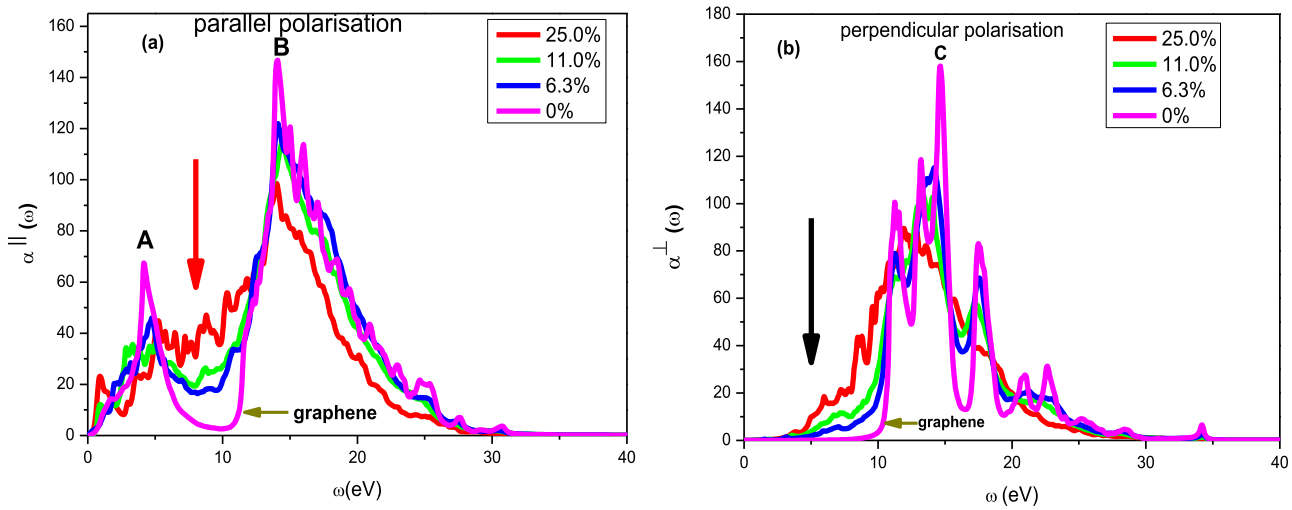

FIG. 7. The anisotropic absorption spectra of graphene (magenta) and Be-S (blue, green, and red colour correspond to a 6.3, 11.0 and 25% impurity concentration) for (a) parallel polarisation and (b) perpendicular polarisation of the electric field vector.

on the absorption of graphene. Next, the influence of the impurity concentration on the absorption spectrum of graphene was considered. As the impurity concentration increases, it is observed that the absorption coefficient of Be-S within 7.0-10.0 eV (see red arrow in Fig. 7 (a)) also increases while the intensity of **A** and **B** peaks not only decreases but slightly redshifted.

For E⊥ as shown in Fig. 7 (b), the graphene spectrum is characterised with one major peak at 14.6 eV, which is due to the $\sigma \rightarrow \pi^*$ interband transition and a featureless region within the interval of 0-10.0 eV. The featureless region is designated with a black arrow, Fig. 7(b). This result with respect to E⊥ is in agreement recent reports on the absorption spectrum of pristine graphene.[16,36,39,42,43] Next, the effect of Be-S atomic pair on the absorption spectrum of graphene was investigated with respect to E⊥. It is found that by increasing the impurity concentration of the Be-S, the absorption coefficient of the system within the interval of 7.0-10 eV (indicated with a black arrow in Fig. 7 (b)) also increases while the intensity of the peak at **C** decreases depending on the amount of the impurity. In summary, it is interesting to mention that under the two different polarisations of the electric field, the absorption coefficient of Be-S in the interval of 7.0-10 eV increases with the impurity concentration. However, the intensity of all the major peaks of the Be-S systems reduces with the increase of the impurity percentage, irrespective of the polarisation field vectors.

F. Electron energy loss spectra (eels)

The eels of graphene and Be-S with different impurity percentage for the $E_{||}$ and E⊥ are shown in Fig. 8. The eels could be defined as the collective excitations of the electrons of a material and computed as the inverse of the dielectric tensors of the systems. In the case of pristine graphene, it has two prominent peaks with respect to $E_{||}$, as shown in Fig. 8 (a). The two peak positions (highlighted as **A** and **B**) which are located at 5.7 and 15-17.0 eV are as a result of the π and the (π+σ) plasmons, respectively. For monolayer graphene, Eberlein *et al.*[44] reported experimental plasmon peaks due to π and (π+σ) as 4.7 and 14.6 eV, respectively. The slight difference between these values and our results might be attributed to the presence of the excitonic effects which is not considered in our computational method. Another interesting feature of the spectrum could be seen as the dip around the 10 eV where the intensity of the system is almost equal to zero (the black arrow in Fig. 8 (a)). As the impurity concentration increases, it could be seen that the intensity of the spectrum in the interval of 7.0-10 eV (indicated with a black arrow in Fig. 8 (a)) also increases. However, the graphene peak at **A** responds differently to the impurity variation. That is, it decreases with the increase in the impurity percentage. For the peak at **B**, it is important to add that there is no significant change that is observed as a result of the change in the impurity concentration.

In the case of E⊥ (Fig. 8 (b)), a prominent resonance peak of graphene is observed at 15.4 eV and the occurrence is because of the transition between filled π and empty π^* bands. It could be seen that the spectrum also has a featureless region with almost zero amplitude within the window of 0–10 eV. It is important to point out that the position of the peak is in accordance with the previous experimental study by T. Eberlein *et al.*[44] Following the analysed eels of graphene, the effect of Be and S atomic pair on the spectrum was investigated. It can be observed that all the amplitude of the peaks of Be-S at approximately 15.4 eV, irrespective of the impurity percentage, is smaller than that of the graphene (Fig. 8 (b)). It is worth mentioning that, as the impurity percentage increases, the behaviour of the spectra of Be-S with respect to E⊥, within 5-10.0 eV, is similar to the ensued response of the material in relation to $E_{||}$. That is, the intensity of Be-S spectra within the region of 5-10.0 eV decreases with the defect concentration.

G. Refractive index (r.i)

Fig. 9 depicts the refractive index spectra of graphene and Be-S with different impurity concentrations with respect to the parallel

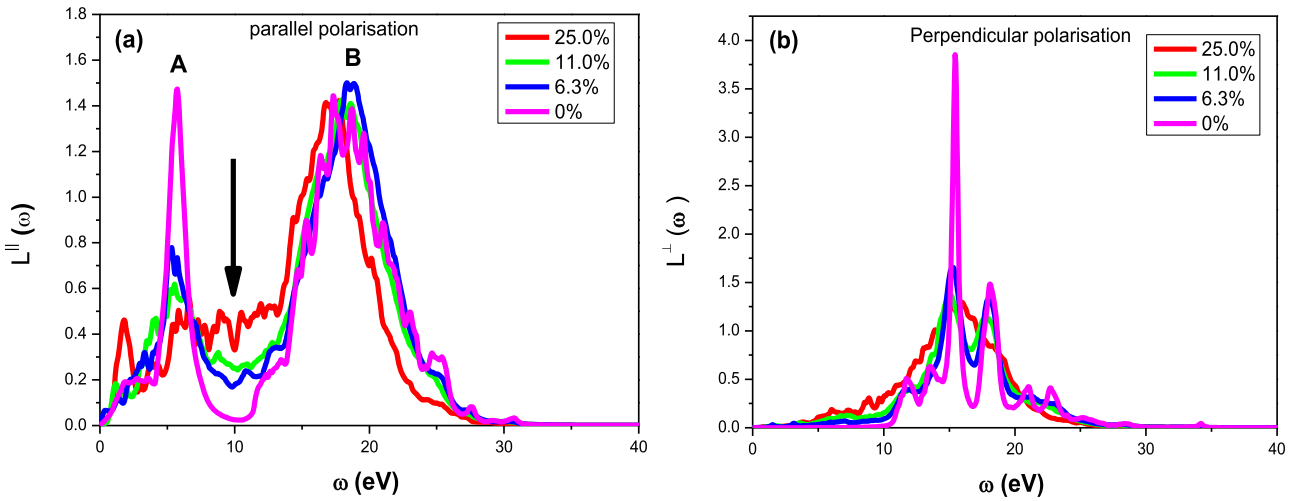

FIG. 8. The anisotropic electron energy loss spectra of graphene (magenta) and Be-S (blue, green, and red colour correspond to a 6.3, 11.0 and 25% impurity concentration) for (a) parallel polarisation and (b) perpendicular polarisation of the electric field vector.

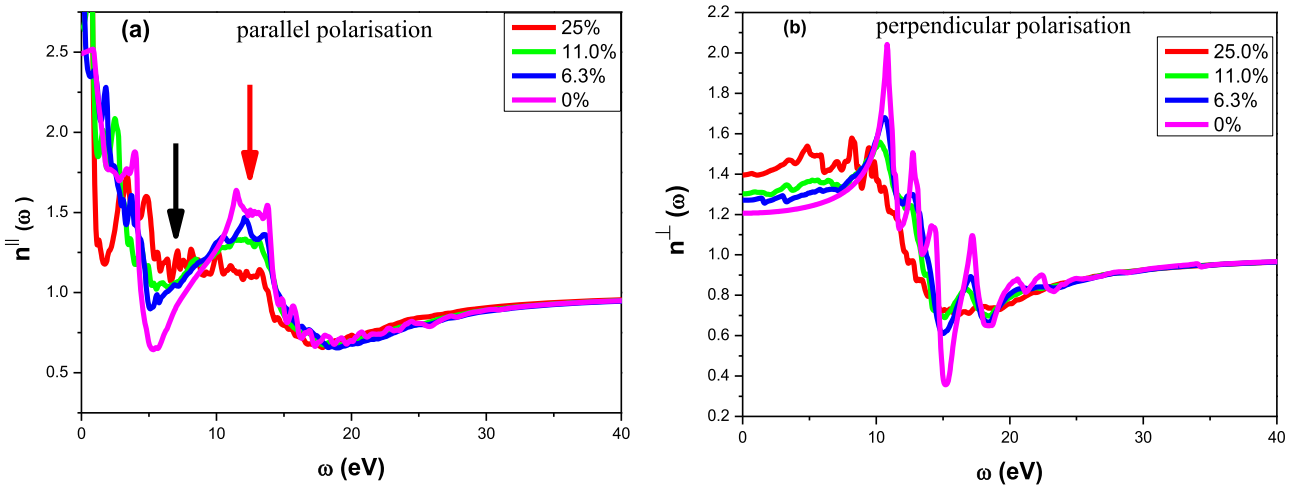

FIG. 9. The anisotropic refractive index spectra of graphene (magenta) and Be-S (blue, green, and red colour correspond to a 6.3, 11.0 and 25% impurity concentration) for (a) parallel polarisation (b) perpendicular polarisation of the electric field vector.

and the perpendicular polarisation of the EM field. In this discussion, only part of the spectra slightly away from the low energy photons has been discussed. Because that region, which is also known as the Drude region, is dominated by the intraband transitions. It is worth reiterating that because of the lack of Drude component in the formulation of the refractive indices, there are inaccuracies in the features of the optical spectra in the low energy region. Based on this account, in relation to $E_{||}$, in Fig. 9 (a), only the dip (black arrow direction) and peak (red arrow direction) of the spectra around 5.0 and 10.0 eV, respectively, have been compared in relation to that of the pristine graphene. As a result, it can be seen that as the impurity concentration increases, both the dip around 5 eV and the peaks at about 10.0 eV of the spectra decreases. However, for $E\perp$ (see Fig. 9 (b)) it is found that the pristine graphene has a maximum peak at 10.0eV and a dip at 15 eV. As the impurity concentration increases, both peaks and the dips of the spectra of the doped systems reduce in comparison to that of the pristine graphene.

H. Reflectivity

Fig. 10 illustrates the reflectivity spectra of graphene and Be-S at different impurity concentrations with respect to (a) the parallel and (b) the perpendicular polarisation of the field vector. For $E_{||}$, as shown in Fig. 10 (a), the pristine graphene is characterised with two major peaks. The maximum peak (indicated as **A**) occurs at 4.3 eV whereas the next peak highlighted as **B** is observed at 14.2 eV. Moreover, the spectrum of the system also has a featureless region of 7.0-10.0 eV which is marked with the arrow in Fig. 10 (a). The peak

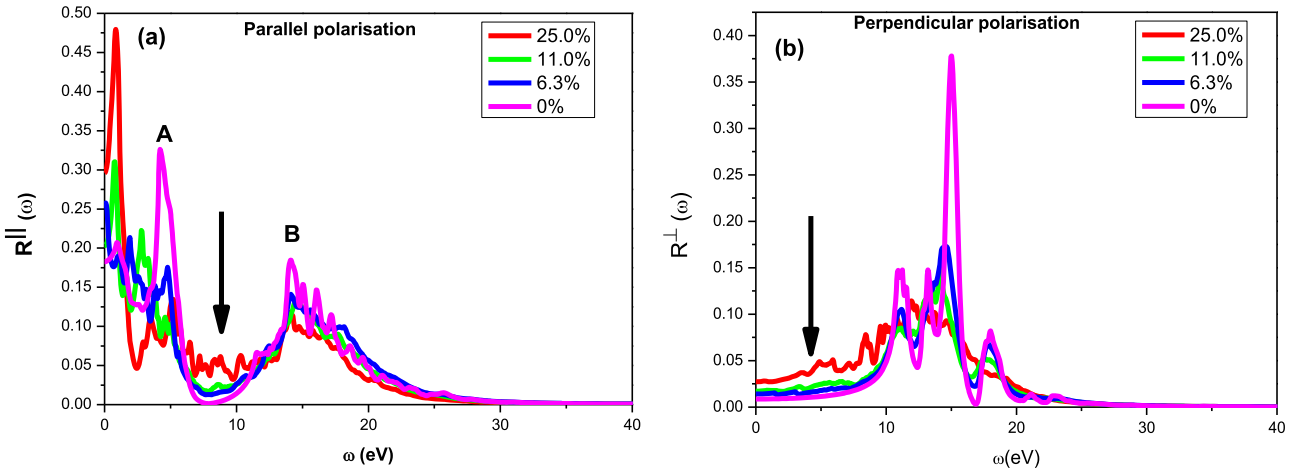

FIG. 10. Shows anisotropic refractivity spectra of graphene (magenta) and Be-S (blue, green, and red colour correspond to a 6.3, 11.0 and 25% impurity concentration) for (a) parallel polarisation (b) perpendicular polarisation of the electric field vector.

positions of this spectrum are in agreement with the recent theoretical studies[15,36] on graphene. For Be-S, as the impurity percentage increases, it can be observed that the amplitude of the optical peak at **A** reduces as well; whereas for the peak at **B**, there is no substantial change in the amplitude. In the interval of 7.0-10 eV, Be-S also has a low value of reflectivity at a relatively small impurity concentration. However, the reflectivity of the system becomes significant as the impurity concentration increases.

In the case of E⊥ (as shown in Fig. 10 (b)), a prominent graphene peak is observed at 15.0 eV while almost zero reflectivity coefficients (indicated with a black arrow) of the spectrum can be noticed within the interval of 0-10 eV. This finding agrees with earlier reports[15,36] on the ab-initio investigation of the optical characteristics of graphene. Next, the effect of Be and S atomic pairs on the reflectivity spectrum of graphene was investigated. Within the interval of 0-10 eV (indicated with a black arrow in Fig. 10 (b)), it is noticeable that the amplitude of the Be-S spectra increases with the impurity concentration. However, for the peak around 15.0 eV, the amplitude decreases with the impurity percentage.

It is worth mentioning that for both $E_{||}$ and E⊥, the pristine graphene has low values of reflectivity and absorption coefficients within the window of 7.0-10 eV. This implies that the system is transparent in that frequency interval which corresponds to the ultraviolet (UV) region of the electromagnetic spectrum. However, for the Be-S the two optical parameter values increase as the impurity percentage increases in the aforementioned photon energy interval. This response of the optical spectrum of graphene to Be and S co-doping shows that the optical properties of the system can be modulated with the impurity concentration.

IV. CONCLUSIONS

Ab-initio calculations, within the DFT, were employed to investigate the dynamic stability, band structure and optical characteristics of Be-S. The phonon spectrum of the system, due to the absence of imaginary mode, reveals that Be-S (with the impurity concentration of 25%) is dynamically stable. While Be and S preferred to co-exist in an out-of-plane conformation in graphene, the defect formation energy of the system demonstrates that the stability of the system decreases with the impurity concentration. The influence of the impurity concentration on the electronic structure of graphene reveals that it could open up a tunable indirect band-gap in the range of 0-0.72 eV as obtained from our hybrid calculations.

The optical parameters such as dielectric function; refractive index, eels, absorption, and reflectivity of the Be-S were also investigated and compared with that of graphene with respect to the two mutual light polarisation directions. For the pristine graphene, the calculated optical parameters were found to agree with the existing data from other reports. In the case of Be-S, the position of the spectra peaks mimic that of the pristine graphene especially at a small impurity percentage within the photon energy window of 2.0–40.0 eV for both polarisation directions of the field vector. However, there are remarkable deviations at a relatively high impurity percentage. That is, the peaks of Be-S co-doped appeared to be redshifted relative to the corresponding peaks of the pristine graphene. Moreover, it is remarkable to notice that the amplitude of the dominant optical peaks of graphene decreases with the amount of the impurity present in the Be-S.

Graphene has vanishing absorption and reflectivity spectra within the interval of 7.0–10.0 eV, and this makes it a transparent material under ultraviolet radiation, irrespective of the orientation of the polarisation vector field to the sample. However, unlike in the case of the pristine graphene, within 7.0–10.0 eV, the coefficients of the two aforementioned optical parameters for Be-S have substantial values which tend to increase with the defect concentration. This reveals that the optical transparency of graphene can be tuned with the atomic pair of Be and S concentration. With the on-going trend of tailoring the optical characteristics of graphene with heteroatoms to satisfy certain applications in nanodevices, the result of this study provides an insight on the expected changes in the electronic and optical properties of graphene if it is co-doped with the atomic pair of the Be and S atom for use in nanoelectronic and optoelectronic devices.

ACKNOWLEDGMENTS

This study is based on the research supported by the South Africa Research Chairs Initiative (SARChl) of the Department of Science and Technology, and National Research Foundation (NRF) of South African (Grant No. 61056). Any opinion, findings and conclusions stated in the article is that of the authors, and NRF does not accept any liability in this regard. The authors wish to thank Prof. Mark Casida and Dr. B. Mutuma for their invaluable suggestions after reading through the manuscript. O. Okikiola wishes to recognize the financial support from the University of Pretoria for his PhD study. The resources and supports from the Centre for High Performance Computing (CHPC), South Africa, are duly acknowledged.

REFERENCES

[1] K. S. Novoselov, A. K. Geim, S. V. Morozov, D. Jiang, M. I. Katsnelson, I. V. Grigorieva, S. V. Dubonos, and A. A. Firsov, Nature **438**, 197 (2005).
[2] J.-H. Chen, C. Jang, S. Xiao, M. Ishigami, and M. S. Fuhrer, Nat. Nanotechnol. **3**, 206 (2007).
[3] S. V. Morozov, K. S. Novoselov, M. I. Katsnelson, F. Schedin, D. C. Elias, J. A. Jaszczak, and A. K. Geim, Phys. Rev. Lett. **100**, 016602 (2008).
[4] D. A. Siegel, C.-H. Park, C. Hwang, J. Deslippe, A. V. Fedorov, S. G. Louie, and A. Lanzara, Proc. Natl. Acad. Sci. **108**, 11365 (2011).
[5] B. Rosenstein, M. Lewkowicz, H. C. Kao, and Y. Korniyenko, Phys. Rev. B - Condens. Matter Mater. Phys. **81**, 1 (2010).
[6] C. Lee, X. Wei, J. W. Kysar, and J. Hone, Science (80-.). **321**, 385 (2008).
[7] A. A. A. A. Balandin, S. Ghosh, W. Bao, I. Calizo, D. Teweldebrhan, F. Miao, and C. N. Lau, Nano Lett. **8**, 902 (2008).
[8] K. S. Novoselov, A. K. Geim, S. V. Morozov, D. Jiang, Y. Zhang, S. V. Dubonos, I. V. Grigorieva, and A. A. Firsov, Science (80-.). **306**, 666 (2004).
[9] P. Avouris, Nano Lett. **10**, 4285 (2010).
[10] A. K. Geim and K. S. Novoselov, Nat. Mater. **6**, 183 (2007).
[11] K. S. K. S. Kim, Y. Zhao, H. Jang, S. Y. Lee, J. M. Kim, J.-H. H. Ahn, P. Kim, J.-Y. Y. Choi, B. H. Hong, K. S. K. S. Kim, J.-H. H. Ahn, P. Kim, J.-Y. Y. Choi, and B. H. Hong, Nature **457**, 706 (2009).
[12] A. Reina, X. Jia, J. Z. Ho, D. Nezich, H. Son, V. Bulovic, M. Dresselhaus, J. Kong, A. Reina, X. Jia, J. Ho, D. Nezich, H. Son, V. Bulovic, M. S. Dresselhaus, and K. Jing, Nano Lett. **9**, 30 (2009).
[13] S. Bae, H. Kim, Y. Lee, X. Xu, J. S. Park, Y. Zheng, J. Balakrishnan, T. Lei, H. Ri Kim, Y. Il Song, Y. J. Kim, K. S. Kim, B. Özyilmaz, J. H. Ahn, B. H. Hong, and S. Iijima, Nat. Nanotechnol. **5**, 574 (2010).
[14] Z. Liu, J. Li, Z.-H. Sun, G. Tai, S.-P. Lau, and F. Yan, ACS Nano **6**, 810 (2012).
[15] P. Nath, S. Chowdhury, D. Sanyal, and D. Jana, Carbon N. Y. **73**, 275 (2014).

[16]P. Rani, G. S. Dubey, and V. K. Jindal, Phys. E Low-Dimensional Syst. Nanostructures **62**, 28 (2014).
[17]P. Nath, D. Sanyal, and D. Jana, Phys. E Low-Dimensional Syst. Nanostructures **56**, 64 (2014).
[18]P. Rani and V. K. Jindal, RSC Adv. **3**, 802 (2013).
[19]S. Mann, P. Rani, R. Kumar, G. S. Dubey, and V. K. Jindal, RSC Adv. **6**, 12158 (2016).
[20]Y. Ferro, N. Fernandez, A. Allouche, and C. Linsmeier, J. Phys. Condens. Matter **25**, 015002 (2013).
[21]S. Ullah, A. Hussain, W. Syed, M. A. Saqlain, I. Ahmad, O. Leenaerts, and A. Karim, RSC Adv. **5**, 55762 (2015).
[22]A. Hussain, S. Ullah, and M. Farhan, RSC Adv. **6**, 55990 (2016).
[23]P. A. Denis, R. Faccio, and A. W. Mombru, ChemPhysChem **10**, 715 (2009).
[24]O. Olaniyan, R. E. Mapasha, D. Y. Momodu, M. J. Madito, A. A. Kahleed, F. U. Ugbo, A. Bello, F. Barzegar, K. Oyedotun, and N. Manyala, RSC Adv. **6**, 88392 (2016).
[25]G. Kresse and J. Hafner, Phys. Rev. B **49**, 14251 (1994).
[26]G. Kresse and J. Hafner, Phys. Rev. B **47**, 558 (1993).
[27]G. Kresse and J. Furthmüller, Comput. Mater. Sci. **6**, 15 (1996).
[28]G. Kresse, Phys. Rev. B **54**, 11169 (1996).
[29]J. P. Perdew, K. Burke, and M. Ernzerhof, Phys. Rev. Lett. **77**, 3865 (1996).
[30]A. V. Krukau, O. A. Vydrov, A. F. Izmaylov, and G. E. Scuseria, J. Chem. Phys. **125**, 224106 (2006).
[31]M. Gajdoš, K. Hummer, G. Kresse, J. Furthmüller, and F. Bechstedt (n.d.).
[32]K. Parlinski, Z. Q. Li, and Y. Kawazoe, Phys. Rev. Lett. **78**, 4063 (1997).
[33]D. R. Cooper, B. D'Anjou, N. Ghattamaneni, B. Harack, M. Hilke, A. Horth, N. Majlis, M. Massicotte, L. Vandsburger, E. Whiteway, and V. Yu, ISRN Condens. Matter Phys. **2012**, 1.
[34]H. Yanagisawa, T. Tanaka, Y. Ishida, M. Matsue, E. Rokuta, S. Otani, and C. Oshima, Surf. Interface Anal. **37**, 133 (2005).
[35]N. Mounet and N. Marzari, Phys. Rev. B - Condens. Matter Mater. Phys. **71**, 1 (2005).
[36]O. Olaniyan, R. E. Maphasha, M. J. Madito, A. A. Khaleed, E. Igumbor, and N. Manyala, Carbon N. Y. **129** (2018).
[37]O. V. Sedelnikova, L. G. Bulusheva, and A. V. Okotrub, J. Chem. Phys. **134**, 244707 (2011).
[38]M. Houmad, H. Zaari, A. Benyoussef, A. El Kenz, and H. Ez-Zahraouy, Carbon N. Y. **94**, 1021 (2015).
[39]V. G. Kravets, A. N. Grigorenko, R. R. Nair, P. Blake, S. Anissimova, K. S. Novoselov, and A. K. Geim, Phys. Rev. B - Condens. Matter Mater. Phys. **81**, 1 (2010).
[40]A. G. Marinopoulos, L. Reining, A. Rubio, and V. Olevano, Phys. Rev. B **69**, 245419 (2004).
[41]L. Yang, J. Deslippe, C.-H. H. Park, M. L. Cohen, and S. G. Louie, Phys. Rev. Lett. **103**, 186802 (2009).
[42]C. Huang, L. Han, L. Wu, R. Su, J. Chen, and P. Lu, Eur. Phys. J. B **88**, 1 (2015).
[43]A. Laref, A. Ahmed, S. Bin-Omran, and S. J. Luo, Carbon N. Y. **81**, 179 (2015).
[44]T. Eberlein, U. Bangert, R. R. Nair, R. Jones, M. Gass, A. L. Bleloch, K. S. Novoselov, A. Geim, and P. R. Briddon, Phys. Rev. B - Condens. Matter Mater. Phys. **77**, 1 (2008).